Improved determination of the $1_0 - 0_0$ rotational frequency of NH_3D^+ from the high resolution spectrum of the ν_4 infrared band

J. L. Doménech, M. Cueto, V. J. Herrero & I. Tanarro

Molecular Physics Department, Instituto de Estructura de la Materia (IEM-CSIC). Serrano 123. 28006 Madrid, Spain

jl.domenech@csic.es

B. Tercero

Department of Astrophysics, CAB. INTA-CSIC. Crta Torrejón-Ajalvir Km 4, 28850 Torrejón de Ardoz. Madrid, Spain

A. Fuente

Observatorio Astronómico Nacional, Apdo. 112, 28803, Alcalá de Henares, Spain

and

J. Cernicharo

Department of Astrophysics, CAB. INTA-CSIC. Crta Torrejón-Ajalvir Km 4, 28850 Torrejón de Ardoz. Madrid, Spain

Received _____; accepted _____

Revised version June 4, 1013

ABSTRACT

The high resolution spectrum of the ν_4 band of NH_3D^+ has been measured by difference frequency IR laser spectroscopy in a multipass hollow cathode discharge cell. From the set of molecular constants obtained from the analysis of the spectrum, a value of 262817 ± 6 MHz ($\pm 3\sigma$) has been derived for the frequency of the $1_0 - 0_0$ rotational transition. This value supports the assignment to NH_3D^+ of lines at 262816.7 MHz recorded in radio astronomy observations in Orion-IRc2 and the cold prestellar core B1-bS.

Subject headings: Molecular data — Line: identification — ISM: molecules — methods: laboratory — techniques: spectroscopic

1. Introduction

The concentrations of ions in interstellar space are typically orders of magnitude lower than those of the most abundant neutral species (Petrie & Bohme 2007, Snow & Bierbaum 2008, Larsson et al. 2012) but, due to the fact that ion-molecule reactions are often barrier-less and have large rate coefficients, ions play a key role in the low-temperature gas phase chemistry of the interstellar medium (ISM) (Watson 1973, Herbst & Klemperer 1973, Herbst 2001). Many of the 20 cations detected up to date in the ISM (Petrie & Bohme 2007, Larsson et al 2012) are protonated derivatives of small molecules that can be formed in chains of proton transfer processes involving molecules with varying proton affinities (PA) (Burt et al. 1970, Carrasco et al. 2012a, Carrasco et al. 2013). The global initiator of these chains is assumed to be H_3^+, the most frequently produced ion in the ISM (Oka 2006), which is readily generated in the collisions of H_2 molecules with H_2^+ ions. Due to the low PA (422.3 kJ mol^{-1}) of the hydrogen molecule (Burt et al. 1970, Hunter & Lias 1998), H_3^+ has a high tendency to transfer a proton and return to H_2. Among the small molecules most common in the ISM (CO, N_2, HCN, H_2O, NH_3, CH_2O, CH_4, CH_3OH), ammonia has the highest proton affinity (PA=853 kJ mol^{-1}) and consequently NH_4^+, once formed, will be stable toward further reactions with the most abundant species. In fact, astrochemical models predict NH_4^+ to become the dominant ion in some warm astronomical environments where NH_3 desorbs from interstellar grains and becomes available for gas phase ion-molecule chemistry (Rodgers & Charnley 2003, Harada et al. 2010, Aikawa et al. 2011). It should be noted that, in spite of the concentration enhancement provided by grain desorption, NH_3 always represents a small fraction of the neutral species inventory. The dominance of NH_4^+ in the ion distributions of laboratory plasmas containing just small fractions of NH_3 has also been experimentally demonstrated (Carrasco et al. 2011, Carrasco et al. 2013).

Interstellar NH_4^+ is not limited to warm environments. It is also assumed to play a

key role in the low temperature gas-phase formation of ammonia in cold clouds (Nejad et al. 1990). In this case, the suggested route starts with the reaction between N^+ and H_2 to yield NH^+ and proceeds through successive hydrogenation steps to the formation of NH_4^+ that transforms into NH_3 through dissociative recombination with electrons. The first step in this route is endoergic for para-hydrogen molecules in their ground state, but slightly exoergic for ortho-hydrogen, and Dislaire et al. (2012) have shown that realistic ortho/para ratios could explain the relative abundances of nitrogen hydrides observed in dark clouds. In general, the high gas-phase chemical stability of NH_4^+ in the ISM, which is mostly destroyed just in collisions with electrons, suggests that it can build up to high concentrations in different astronomical environments and, given its paramount importance for nitrogen chemistry in space, it is a desired goal for astronomical searches. Unfortunately, NH_4^+ is a spherical top molecule with no permanent electric dipole moment and thus unsuitable for radioastronomic observation. As far as we know, the ion has never been detected in the ISM. However, deuterated variants of NH_4^+ do possess a permanent dipole moment and could, in principle, be observed. Variously deuterated ammonia molecules, likely related to deuterated ammonium, are observed in dense cores, where fractionation leads to an enhancement of the molecular deuterium content (Roueff et al. 2005) and, in particular, all deuterated isotopologues of NH_3 have been detected in the cold prestellar cloud B1-bS (Lis et al. 2002).

Spectroscopic data useful for astronomic observations are available for the monodeuterated ammonium ion. Specifically, a frequency of 262807 ± 9 MHz ($\pm 3\sigma$) was predicted by Nakanaga & Amano (1986, hereafter N&A (1986)) for the $1_0 - 0_0$ transition of NH_3D^+. This value was derived using the ground-state molecular constants obtained by those authors from their high resolution spectroscopic measurements of the ν_4 infrared band of the ion. Recent work by Cernicharo et al. (2013, accompanying letter) has established the presence of an emission line at 262816.7 MHz in Orion-IRc2 and in B1-bS.

The frequency is approximately 10 MHz higher than that estimated by Nagaka and Amano for monodeuterated ammonium and thus exceeds slightly the 3σ uncertainty of the spectroscopic value, strongly suggesting that the feature can correspond to this species. In the present work we have refined the previous spectroscopic measurements of N&A (1986) further constraining the frequency of the $1_0 - 0_0$ transition and providing additional support for the assignment of the observed 262816.7 MHz emission feature to the presence of NH_3D^+.

2. Experimental details

The experimental setup used in this work is similar to that described elsewhere (Tanarro et al. 1994a, 1994b). It consists of an IR difference-frequency laser spectrometer (Doménech 1990, Bermejo et al. 1989), and a hollow cathode discharge reactor refrigerated by room-temperature water, with multipass optics in a White cell configuration, similar to the design of Foster & McKellar (1984).

The IR radiation is generated by difference-frequency mixing, following the scheme of Pine (1974), of an Ar^+ laser and a tunable ring dye laser in a $LiNbO_3$ crystal. Tuning the dye laser, while keeping the Ar^+ laser frequency locked, tunes the IR frequency, which is the difference between that of the Ar^+ laser and that of the ring dye laser. In our experiment, the Ar^+ laser is frequency locked to a hyperfine transition of $^{127}I_2$, (a_3 component of the P(13) $43 - 0$ transition, known with an accuracy ~ 0.1 MHz, (Quinn 2002)) and has a residual frequency jitter less than 1 MHz and long-term stability of the same order of magnitude. The wavelength of the ring dye laser (also frequency stabilized, with a residual jitter of ~ 3 MHz) is measured in just 1 ms at each data point of the spectrum by a high accuracy wavemeter based on Fizeau interferometers (High Finesse WSU10) with a manufacturer-stated absolute accuracy of better than 10 MHz (3σ). The Ar^+ laser is

used to calibrate the wavemeter and thus insure its accuracy throughout the experiments. The linewidth of the IR beam is the combined linewidth of those of the visible lasers, i.e. ~ 3 MHz. The internal coherence of the infrared frequency scale is limited by that of the wavemeter. From repeated measurements of N_2O lines in the $3300 - 3400$ cm^{-1} region, and their comparison with the values in the HITRAN 2008 database (Rothman et al. 2009, Toth (2004)), we have verified a reproducibility and internal coherence of our IR frequency scale better than 1.2×10^{-4} cm^{-1} (4 MHz) rms and a systematic offset of 6×10^{-4} cm^{-1} (18 MHz), which is within the combined uncertainty of the wavemeter and the quoted uncertainty limits for those line frequencies in HITRAN ((1-10)$\times10^{-4}$ cm^{-1}, or $3 - 30$ MHz).

The IR beam traverses the multipass cell 12 times, giving an effective absorption length of 9 meters inside the discharge. In order to improve the detection sensitivity, both the IR beam and the discharge are amplitude-modulated, at 14.2 and 5.5 kHz, respectively, and the IR signal is detected by an InSb detector connected to a dual-phase lock-in whose reference frequency is the sum of the other two (i.e. 19.7 kHz). In this way, only changes in the IR beam intensity, due to species whose concentration is modulated in the discharge, are detected. The three frequencies are derived from a common oscillator by appropriately chosen integer dividers (Domingo et al. 1994), therefore, insuring phase stability between the three of them. The detection time constant is 100 ms with 12 db/oct roll off. The ring dye laser scans at 0.005 cm^{-1}s^{-1} rate. Each line has been recorded 10 times and the results averaged in a grid spaced 0.001 cm^{-1}.

The discharge is modulated at 5.5 kHz through an audio amplifier, a step-up transformer and a circuit designed to avoid the transformer core saturation, since the hollow cathode discharge acts inherently as an electric rectifier. Typical discharge conditions are 200 mA and 400 V rms. The relatively high modulation frequency has been chosen to favor the detection of ionic species, whose lifecycles follow closely the on-off condition of

the discharge, and to minimize undesired absorption signals associated with much slower processes like concentration change of the neutral species caused by multistep wall reactions (Carrasco et al. 2012b, 2013). Nevertheless, we have observed spectral signatures from NH_3 due to a combination of population and Doppler width changes that occur with the small temperature change on the "on" periods of the discharge, similar to those observed in Tanarro et al. (1994a) for other stable species. Note that the kinetic temperature deduced from the observed Doppler widths of the ions is ~ 315 K, i.e. very near the temperature of the refrigerated cathode.

A 32 Pa (0.32 mbar) gas flowing mixture of NH_3 (37%) + D_2 (63%) is used in the discharge as plasma precursor. Gas flows, measured with rotameters at 5×10^4 Pa (500 mbar) absolute input pressure, were 15 ml/min and 30 ml/min for NH_3 and D_2, respectively. In the hollow cathode discharges used, efficient atomic recycling at the metallic cathode wall (Jiménez-Redondo et al. 2011, Carrasco et al. 2011) leads to an extensive isotopic scrambling both in the neutrals and ions. Most of the initial NH_3 is transformed into N_2 and H_2 and the pressure raises to ~ 46 Pa (~ 0.46 mbar). The mixture proportions, flow rate and pressure were empirically selected to maximize the NH_3D^+ concentration.

Although the ion concentrations have not been directly measured in the present experiment, previous kinetic studies and Langmuir probe measurements by our group (Carrasco et al. 2011, Carrasco et al. 2013) on comparable hollow cathode discharges of H_2/N_2 mixtures, indicate that the ion distributions in our cell should be dominated by NH_4^+, with smaller concentrations of N_2H^+ and H_3^+ (and their deuterated variants) and that the total ion densities should be of the order of $\sim (1-5)\times 10^{10}$ cm^{-3}, with electron temperatures of $\sim 3.0 \pm 0.5$ eV. These density values are also consistent with estimates made from the measured cathode current and glow region dimensions using Bohm's velocity (Lieberman & Lichtenberg 1994). The concentrations of the main individual ions and, in

particular, of NH_3D^+ are estimated to be in the $10^9 - 10^{10}$ cm $^{-3}$ range.

It must be noted that this set-up is very similar to the one used by N&A (1986). The main differences between them are: the IR frequency measuring system (a high accuracy wavemeter for the dye laser in our case, and calibration with N_2O IR absorption lines with 1×10^{-3} cm^{-1} (30 MHz) accuracy in the previous work), the detection scheme at the sum frequency vs. detection at the discharge frequency, the different frequencies of the discharge (5.5 kHz vs. 17 kHz), the rather different proportion of NH_3 and D_2 in the gas mixture ($\sim 1:2$ in our case vs. 1:10 in the previous work), the different absorption path lengths (9 m in this work vs. 20 m in the previous one) and the IR power available (~ 1 μW in this work vs. ~ 10 μW in the previous one). We would like to emphasize that our experiment has been guided and facilitated extensively by the previous study of N&A (1986). The major experimental improvement of the present study is due to the availability of a more precise frequency scale and a more favorable ratio of precursors in the discharge.

3. Results and discussion

We have recorded 114 lines between 3268.4 and 3414.7 cm^{-1}. Not all the spectral interval has been scanned. Instead, we have chosen to scan selected regions around the line frequencies calculated with the constants provided by N&A (1986). In each region, 10 recordings have been made and averaged, in order to improve the signal to noise ratio. From the repeatability of the shape of the most intense lines, and from the fact that no broadening is observed in the averages, we are assured that the frequency scale derived from the wavemeter is highly reproducible. The predictions, new assignments and fits have been made with the help of the PGOPHER program (Western 2010). A ~ 1 cm^{-1} wide region of the spectrum in the central part of the band is shown in Figure 1, which can be compared with Figure 1 of N&A (1986). The more prominent features are due to NH_4^+, which we have

identified throughout the spectrum with the measurements and predictions of Schäfer et al. (1984). Our more favorable intensity ratio between NH_3D^+ and NH_4^+ signals as compared with those of N&A (1986) is worth noting. Figure 2 shows some more examples of more isolated lines of NH_3D^+ in the P- and R- regions.

Each averaged line has been fit to a Gaussian function, to derive its line center. Standard deviations of the center frequency derived from these fits are $(1-4)\times10^{-4}$ cm^{-1} ($3-12$ MHz). The line center frequencies have been fit to the same Hamiltonian used in the work of N&A (1986), with the only exception of the sign of the q_+ (rotational l-doubling) parameter, since PGOPHER uses the opposite sign convention for it in its matrix elements. For completeness, we give here the expressions used for the energy levels, which are common for a prolate symmetric-top. For the nondegenerate ground-state, ignoring spin-rotation effects:

$$\begin{aligned} &E''(J,K) = \\ &B''J(J+1) + (A''-B'')K^2 \\ &- D''_J J^2(J+1)^2 - D''_{JK}J(J+1)K^2 - D''_K K^4 \\ &+ \text{higher order centrifugal distortion terms,} \end{aligned} \tag{1}$$

and for the degenerate $v_4 = 1$ state

$$\begin{aligned} &E'(J,k) = \nu_0 \\ &+ B'J(J+1) + (A'-B')k^2 \\ &+ (-2A'\zeta + \eta_J J^2 + \eta_K k^2)lk \\ &- D'_J J^2(J+1)^2 - D'_{JK}J(J+1)k^2 - D_K k^4 \\ &+\text{higher order centrifugal distortion terms,} \end{aligned} \tag{2}$$

with the off-diagonal matrix elements, responsible for the rotational l-doubling,

$$\begin{aligned} &\langle J,k+2,l+1|H|J,k,l-1\rangle = \tfrac{1}{2}q_+[(J(J+1) \\ &-k(k-1))(J(J+1)-k(k+1))]^{\frac{1}{2}} \end{aligned} \tag{3}$$

A and B are the rotational constants perpendicular and parallel, respectively, to the symmetry axis. The D constants account for the centrifugal distortion effects. J and K are the usual rotational quantum numbers, with $K = |k|$. Recall that Coriolis interaction splits $k \neq 0$ levels in the degenerate vibrational state into $+l$ and $-l$ levels (involving the parameters ζ, η_J and η_K above) and that the $(\Delta k = \pm 2, \Delta l = \pm 2)$ interaction splits the $k = l = \pm 1$ levels into pairs (involving the q_+ parameter). For a more detailed description of the vibration-rotation Hamiltonian and the matrix elements used here the reader is referred to Papousek & Aliev (1982) and PGOPHER's documentation (Western 2010), respectively.

Finally, 76 lines have been fitted, 15 more than in the N&A (1986) work. The lines that have not been included in the fit either show interference from NH_4^+ or NH_3 features, have very poor signal to noise ratio, or show abnormally high linewidth (indicating a possible overlap). Besides, we have restricted ourselves mostly to lines with $J, K \leq 7$, in order to avoid using sextic and higher centrifugal distortion constants. Restriction to these quantum numbers, even at the expense of reducing the number of observations included in the fit, provides a better description of the low lying levels that we pursue, avoiding the correlations between parameters that appear as the number of degrees of freedom is increased without a much larger number of observations.

Table 1 shows the observed frequencies, observed minus calculated residuals and the assignments of the fitted lines. The standard deviation of the fit is $5{\times}10^{-4}$ cm^{-1}. Table 2 shows the resulting constants and their standard deviations (1σ) derived from the fit. Since ν_4 is a perpendicular band of a symmetric top, A'', A', D''_K, D'_K and ζ cannot be independently determined from the observations, so A'' and D''_K have been constrained to the same values as in the N&A (1986) paper. As indicated there, this choice of parameters affects ν_0, ζ, A$'$ and D'_K values, while the rest remain unaffected. Specifically, the frequency of the $J_K = 1_0 - 0_0$ pure rotational transition, namely $2B'' - 4D''$, does not depend on

any of these parameters, so our estimation is not influenced by the constraints. Table 2 also shows the results from N&A (1986), showing that the most significant changes are in the B and D rotational constants. From the B'' and D''_J values, we obtain a frequency for the $1_0 - 0_0$ transition of 262816.8 MHz, in good agreement with the observation of Cernicharo et al. (2013, accompanying letter). We are aware that the near perfect match is probably fortuitous, given the precision of the individual IR frequencies and the statistical uncertainty of the parameters derived from the fit.

In order to summarize, based on our observations and the analysis described above, we propose a value of 262817 ± 6 MHz ($\pm 3\sigma$) for the frequency of the $1_0 - 0_0$ pure rotational transition of NH_3D^+. Our IR measurements improve upon those of N&A (1986) thanks to a more precise frequency scale and a larger number of observed lines. This frequency is in good agreement with that of the feature detected in Orion-IRc2 and B1-bS (Cernicharo el al. 2013, accompanying letter), thus supporting the identification of NH_3D^+ in the ISM.

The authors acknowledge the support from the Spanish MICINN through grant CSD2009-00038. JLD acknowledges additional financial support through grant FIS2012-38175; VJH and IT acknowledge additional financial support through grant FIS2010-16455; BT and JC acknowledge additional financial support through grant AYA2009-07304. JC thanks U. Paris Est for an invited professor position during the completion of this work. Our skilful technicians M. A. Moreno, and J. R. Rodríguez are gratefully acknowledged.

REFERENCES

Aikawa, Y., Furuya, K., Wakelam, V. et al. 2011, in IAU Symp. 280, The Molecular Universe, ed. J. Cernicharo & R. Bachiller, (Cambridge: Cambridge University Press), 33

Bermejo, D., Domenech, J. L., Cancio, P., Santos, J., Escribano, R., 1989, in Proc. of the IX Conf. on Laser Spectroscopy, Laser Spectroscopy IX, ed. Feld, M.S., Thomas J.E. & Mooradian, A. (San Diego: Academic Press),126

Burt, J. A., Dunn, J. L., McEwan, M. J. et al. 1970, J. Chem. Phys. 52, 6062

Carrasco, E., Jiménez-Redondo, M., Tanarro, I., Herrero, V. J., 2011, Phys. Chem. Chem. Phys., 13, 19561

Carrasco, E., Herrero, V. J., Tanarro, I., 2012a, J. Phys. D: Appl. Phys., 45, 305201

Carrasco, E., Jiménez-Redondo, M., Tanarro, I., Herrero, V. J., 2012b, PPCF 54, 124019

Carrasco, E., Tanarro, I., Herrero, V. J., Cernicharo, J., 2013, Phys. Chem. Chem. Phys., 15, 1699.

Cernicharo, J., Tercero, B., Fuente. A, Domenech, J. L., Cueto, M. et al. 2013, ApJL, (accompanying letter)

Dislaire, V., Hily-Blant, P., Faure, A., et al., 2012, A&A 537, A20

Doménech, J.L. 1990, Espectroscopía infrarroja de muy alta resolución. PhD Thesis, Madrid: Universidad Complutense, http://hdl.handle.net/10261/76991

Domingo, C., Tanarro, I., Sanz, M. M., et al. 1994, Proceedings of SPIE, 2124, 227

Foster, S. C., McKellar, A. R. W. 1984, J. Chem. Phys. 81, 3424

Harada, N., Herbst, E., & Wakelam, V. 2010, ApJ, 721, 1570

Herbst, E. 2001, Chem. Soc. Rev. 30, 168

Herbst, E. & Klemperer, W. 1973, ApJ, 185, 505

Hunter, E. P. L.& Lias, S. G. 1998, J. Phys. Chem. Ref. Data, 27, 413

Jiménez-Redondo, M., Carrasco, E., Herrero, V. J. & Tanarro I. 2011, Phys. Chem. Chem. Phys. 13, 9655

Larsson, M., Geppert, W. D. & Nyman G., 2012, Rep. Prog. Phys. 75, 066901

Lieberman, M. A. & Lichtenberg, A. J. 1994, Principles of plasma discharges and materials processing (New York: Wiley & Sons)

Lis, D. C., Roueff, E., Gerin, M. et al. 2002, ApJ 571, L55

Nakanaga, T., Amano, T., 1986, Can. J. Phys. 64, 1356

Nejad, L. A. M., Willams, D. A. & Charnley, S. B., 1990, MNRAS, 246, 183

Oka, T. 2006, PNAS, 103, 12235

Papoušek, D. & Aliev, M.R. 1982, Molecular Vibrational/Rotational Spectra, Amsterdam: Elsevier Scientific.

Pine, A. S. 1074, JOSA, 64, 1683

Petrie, S. & Bohme, D. K. 2007, Mass Spectrom. Rev. 26, 258

Schäfer, E., Saykally, R. J. & Robiette, A. G. 1984, JChPh 80, 3969

Snow, T.P. & Bierbaum, V. 2008, ARAC, 1, 229

Rodgers, S.D. & Charnley, S. S. 2003, ApJ, 585, 355

Roueff, E., Lis, D. C., van der Tak, F. F. S., et al. 2005, A&A, 438, 585

Western, C. M. (2010), PGOPHER, a Program for Simulating Rotational Structure (2010, v 7.1.108). University of Bristol, http://pgopher.chm.bris.ac.uk

Quinn, T. J., 2003, Metrologia 40, 103

Rothman L. S., Jacquemart, D., Barbè, A. et al. 2009, J. Quant. Spectrosc. Radiat. Transfer, 110, 533

Tanarro, I., Sanz, M. M., Bermejo, D., Domingo, C., Santos, J., 1994a, J. Chem. Phys., 100, 238

Tanarro, I., Sanz, M. M., Domingo, C., et al. 1994b, J. Phys. Chem., 98, 5862

Toth, R.A., 2004, http://mark4sun.jpl.nasa.gov/n2o.html

Watson, W. D. 1973, ApJ 183, L17

Table 1. Fitted lines, residuals after the fit and the quantum numbers assignment.

$\nu_{\rm obs}/{\rm cm}^{-1}$	(o-c)[a]	J'	K'	l	J''	K''
3275.00762	1.2	5	5	-1	6	6
3277.36239	6.3	5	4	-1	6	5
3279.75397	4.3	6	1	1	7	0
3281.97669	1.2	5	2	-1	6	3
3284.24462	-0.6	5	1	-1	6	2
3286.24996	-7.2	4	4	-1	5	5
3286.48992	-2.0	5	0		6	1
3288.58604	4.2	4	3	-1	5	4
3288.71980	3.2	5	1	1	6	0
3290.89042	-1.4	4	2	-1	5	3
3293.16846	-3.7	4	1	-1	5	2
3297.46387	0.7	3	3	-1	4	4
3299.77847	-0.8	3	2	-1	4	3
3302.06568	4.4	3	1	-1	4	2
3306.56586	6.1	3	1	1	4	0
3310.93202	2.8	2	1	-1	3	2
3313.19858	2.9	2	0		3	1
3315.44070	1.7	2	1	1	3	0
3319.76669	3.7	1	1	-1	2	2
3322.03737	5.4	1	0		2	1
3330.84074	6.5	0	0		1	1
3334.30357	-7.6	6	2	-1	6	3

Table 1—Continued

$\nu_{\rm obs}/{\rm cm}^{-1}$	(o-c)[a]	J'	K'	l	J''	K''
3334.68004	-9.7	4	2	-1	4	3
3334.81962	-1.3	3	2	-1	3	3
3336.32317	5.3	7	1	-1	7	2
3336.57102	2.0	6	1	-1	6	2
3336.96581	-8.1	4	1	-1	4	2
3337.11283	5.2	3	1	-1	3	2
3338.81264	3.3	6	0		6	1
3339.03585	-7.1	5	0		5	1
3339.22520	1.5	4	0		4	1
3339.37658	-3.1	3	0		3	1
3339.49136	-0.3	2	0		2	1
3339.56780	-2.2	1	0		1	1
3341.02311	-0.8	6	1	1	6	0
3341.25759	0.8	5	1	1	5	0
3341.45410	-2.9	4	1	1	4	0
3341.61294	-0.1	3	1	1	3	0
3341.73208	-4.0	2	1	1	2	0
3342.63625	-6.3	8	2	1	8	1
3342.94920	0.8	7	2	1	7	1
3343.22602	6.0	6	2	1	6	1
3343.46451	-0.2	5	2	1	5	1
3343.66511	-3.0	4	2	1	4	1

Table 1—Continued

$\nu_{\rm obs}/{\rm cm}^{-1}$	(o-c)[a]	J'	K'	l	J''	K''
3343.82666	-5.2	3	2	1	3	1
3345.11471	3.2	7	3	1	7	2
3345.39715	-1.2	6	3	1	6	2
3345.64164	-4.0	5	3	1	5	2
3345.84661	-10.1	4	3	1	4	2
3346.01221	-9.4	3	3	1	3	2
3347.25607	-5.2	7	4	1	7	3
3347.54483	1.6	6	4	1	6	3
3347.79345	-4.4	5	4	1	5	3
3348.00364	4.6	4	4	1	4	3
3350.57916	-6.1	1	1	1	0	0
3359.26698	6.9	2	1	1	1	0
3361.47942	-8.8	2	2	1	1	1
3367.91091	-0.9	3	1	1	2	0
3370.12020	-0.8	3	2	1	2	1
3372.30329	-3.2	3	3	1	2	2
3376.51343	4.9	4	1	1	3	0
3378.71679	7.8	4	2	1	3	1
3380.89518	4.8	4	3	1	3	2
3383.04468	3.0	4	4	1	3	3
3385.07123	-1.3	5	1	1	4	0
3387.26751	7.7	5	2	1	4	1

Table 1—Continued

$\nu_{\rm obs}/{\rm cm}^{-1}$	(o-c)[a]	J'	K'	l	J''	K''
3389.44028	4.5	5	3	1	4	2
3391.58446	1.2	5	4	1	4	3
3393.58543	-2.2	6	1	1	5	0
3393.69878	6.8	5	5	1	4	4
3400.07709	0.8	6	4	1	5	3
3402.05462	-7.8	7	1	1	6	0
3408.26843	5.6	8	0		7	1
3408.52168	-3.1	7	4	1	6	3
3410.62517	5.8	7	5	1	6	4
3414.72838	-2.9	7	7	1	6	6

[a](o-c)=$(\nu_{\rm obs} - \nu_{\rm calc})/10^{-4}$ ${\rm cm}^{-1}$

Table 2. Constants derived from the fit

Constants /cm^{-1}	This work	N&A (1986)
A''	5.852[a]	5.852[a]
B''	4.3834351(294)	4.38327(5)
D''_J	$6.1363(373)\times10^{-5}$	$5.87(9)\times10^{-5}$
D''_{JK}	$1.4689(293)\times10^{-4}$	$1.52(6)\times10^{-4}$
D''_K	0.0[a]	0.0[a]
ν_0	3341.07498(17)	3341.0764(3)
A'	5.818834(37)	5.81871(9)
B'	4.3640729(278)	4.36391(5)
D'_J	$5.4024(339)\times10^{-5}$	$5.13(10)\times10^{-5}$
D'_{JK}	$9.705(296)\times10^{-5}$	$1.02(7)\times10^{-4}$
D'_K	$3.801(91)\times10^{-5}$	$3.1(3)\times10^{-5}$
ζ	0.0582020(76)	0.058191(14)[b]
η_J	$-4.2581(686)\times10^{-4}$	$-4.23(13)\times10^{-4}$
η_K	$1.744(74)\times10^{-4}$	$1.76(18)\times10^{-4}$
q_+	$-3.393(98)\times10^{-4}$[c]	$2.93(19)\times10^{-4}$

[a]Constrained in the fit

[b]Calculated from the values of A′ and A′ζ given

in N&A (1986)

[c]Sign convention is opposite to that of N&A (1986)

Note. — Numbers in parentheses are one standard deviation in units of the last quoted digit, as derived from the fit. For this work we give all the significant digits necessary to reproduce the calculated line frequency values.

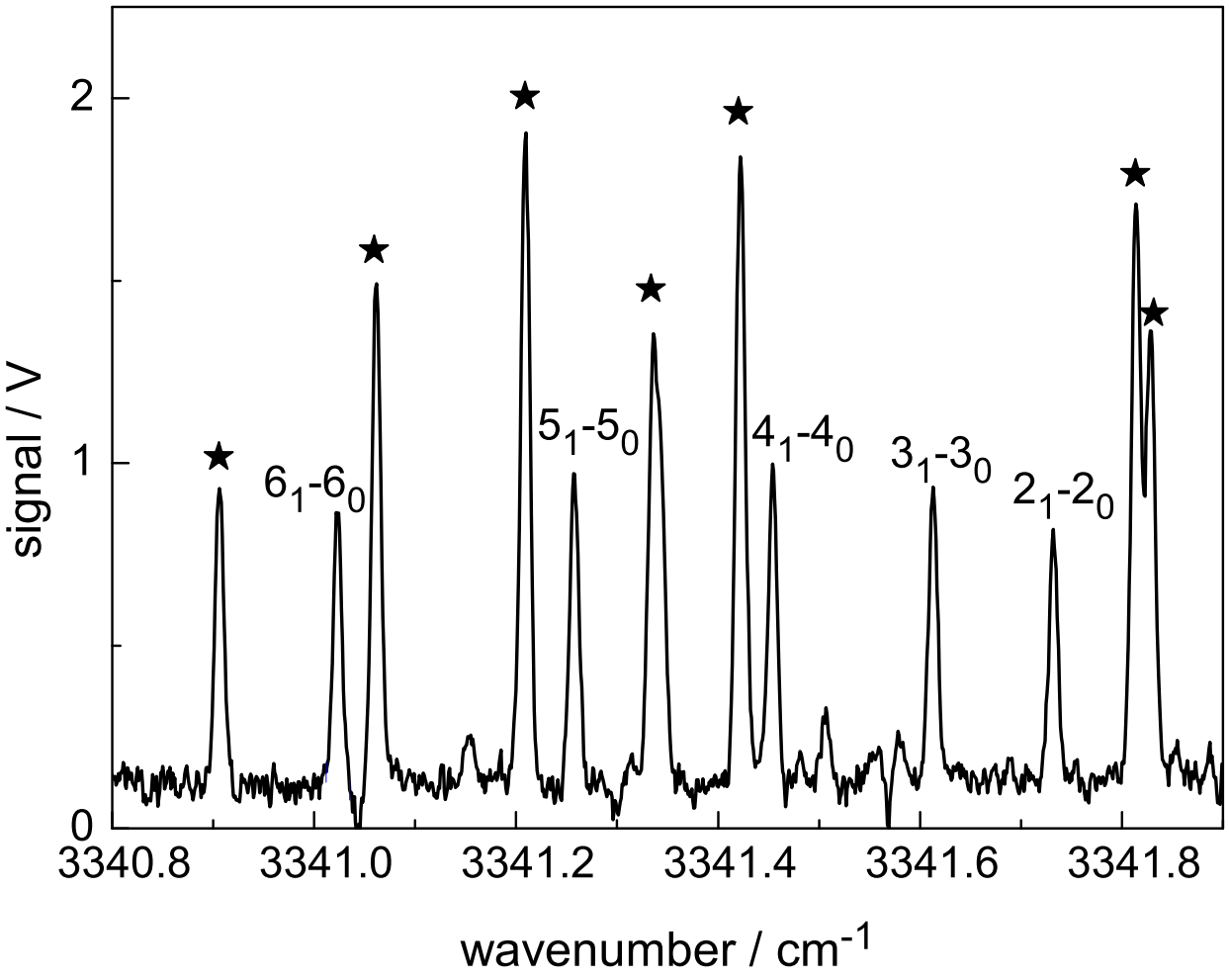

Fig. 1.— Portion of the ν_4 band of NH_3D^+ near the band center. The labeled lines belong to the $(J, K' = 1) \leftarrow (J, K'' = 0)$ progression ($^rQ_0(J)$ in branch notation), and are the same as those shown in Figure 1 of N&A (1986). Lines marked with an asterisk belong to NH_4^+.

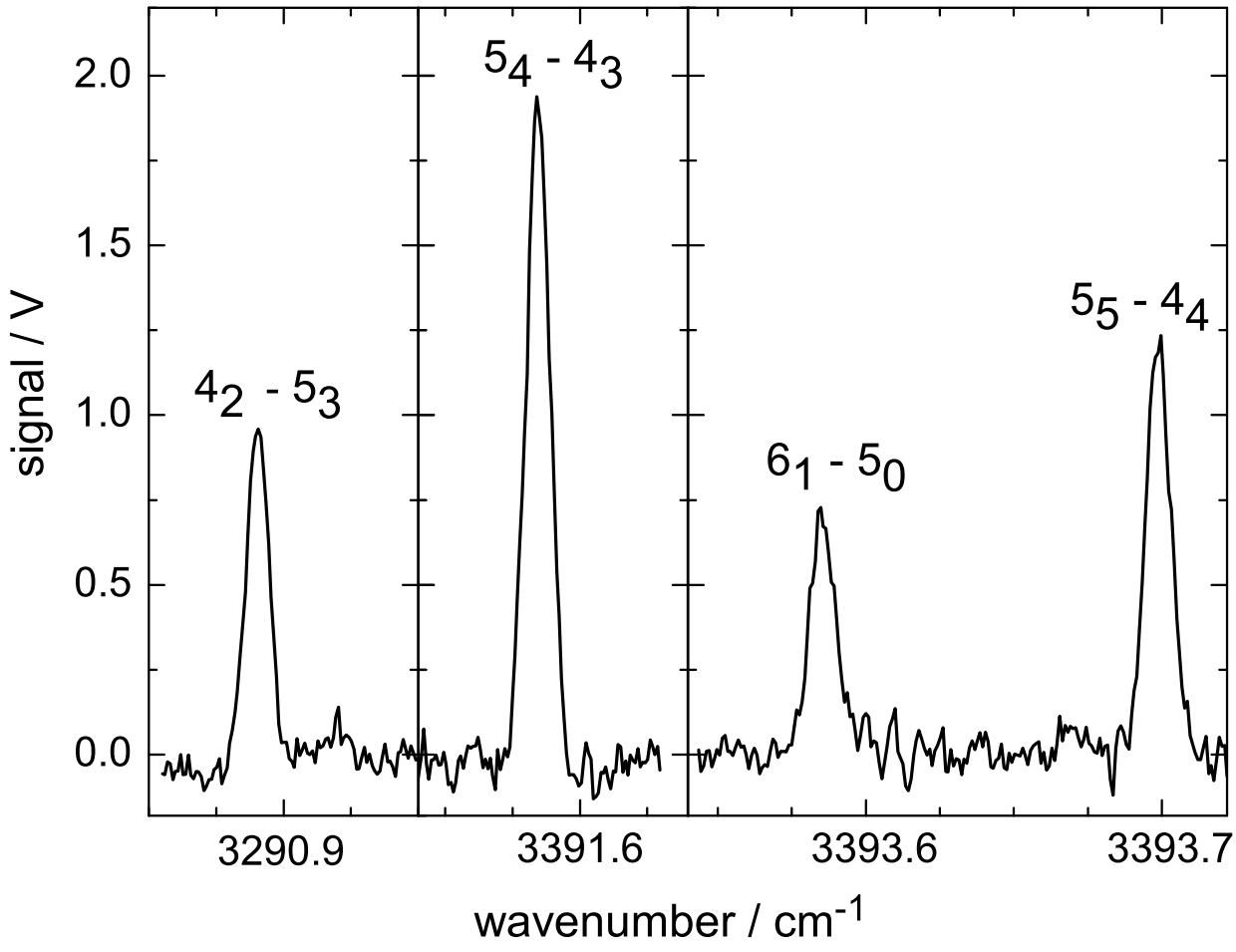

Fig. 2.— Additional examples of ν_4 lines recorded in this work. One horizontal division is 0.025 cm^{-1}.